Geophysical Research Letters

RESEARCH LETTER
10.1029/2018GL077960

Key Points:
- GPS-IR successfully retrieves ground uplifts during snow-free days in freezing season in a continuous permafrost area
- GPS-IR can provide daily records that show a cyclic pattern of thaw subsidence and freezing uplift
- A new composite model incorporating thaw and freeze indices can quantitatively explain the retrieved cyclic elevation changes

Supporting Information:
- Supporting Information S1
- Figure S1
- Figure S2
- Figure S3

Correspondence to:
Y. Hu and L. Liu,
liulin@cuhk.edu.hk;
yfhu@whu.edu.cn

Citation:
Hu, Y., Liu, L., Larson, K. M., Schaefer, K. M., Zhang, J., & Yao, Y. (2018). GPS interferometric reflectometry reveals cyclic elevation changes in thaw and freezing seasons in a permafrost area (Barrow, Alaska). *Geophysical Research Letters*, *45*. https://doi.org/10.1029/2018GL077960

Received 17 MAR 2018
Accepted 23 MAY 2018
Accepted article online 30 MAY 2018

GPS Interferometric Reflectometry Reveals Cyclic Elevation Changes in Thaw and Freezing Seasons in a Permafrost Area (Barrow, Alaska)

Yufeng Hu[1,2], Lin Liu[1], Kristine M. Larson[3], Kevin M. Schaefer[4], Jiahua Zhang[1], and Yibin Yao[2]

[1]Earth System Science Programme, Faculty of Science, The Chinese University of Hong Kong, Hong Kong, China, [2]School of Geodesy and Geomatics, Wuhan University, Wuhan, China, [3]Department of Aerospace Engineering Sciences, University of Colorado Boulder, Boulder, CO, USA, [4]National Snow and Ice Data Center, Cooperative Institute for Research in Environmental Sciences, University of Colorado Boulder, Boulder, CO, USA

Abstract Ground surface over permafrost area undergoes seasonal subsidence and uplift caused by the annual thawing and freezing of the active layer. Applying the Global Positioning System (GPS) interferometric reflectometry technique to the signal-to-noise ratio data collected by a continuously operating GPS station in a permafrost area in Barrow, we retrieve the daily surface elevation changes on snow-free days over a decade (2007–2016). Among these years, 2016 had the longest snow-free season, offering the longest and most complete records of elevation changes. Use this year as an example, we show that the ground subsided in thaw season and then uplifted from September to early November (freezing season) with an amplitude of 5.1 ± 0.2 cm. We also develop a composite model that includes both thaw and freeze indices to characterize the cyclic movements. Our composite model effectively explains the observed cyclic elevation changes and could be used in other permafrost studies.

Plain Language Summary The ground surface over permafrost area subsides and uplifts annually associated with the thawing and freezing processes. We obtain continuous records of elevation changes during snow-free days using reflected Global Positioning System (GPS) signals. Our new measurements reveal the cyclic pattern of subsidence and uplift, which is successfully quantified by a new and simple model that accounts for both thawing and freezing. These observations are important for a quantitative understanding of the progressive movements of frozen ground and for assessing the impact of elevation changes on natural environments and infrastructure over permafrost areas.

1. Introduction

Permafrost is defined as the ground that remains at or below 0 °C for at least two consecutive years. On top of the permafrost is the active layer that thaws and freezes annually. Due to the cyclic phase changes of water within the active layer, the ground surface subsides and uplifts when the active layer thaws and freezes. Continuous observations of cyclic elevation changes during the thaw-freeze cycle are important for a quantitative understanding of the progressive dynamics of frozen ground and for assessing the impact of elevation changes on local or regional hydro-ecological systems and human infrastructures over permafrost areas.

Various strategies and instruments have been developed for measuring elevation changes in permafrost areas. In situ mechanical methods use specially designed markers or devices such as telescoping tubes, magnet probes, and bedsteads to measure heave or settlement (Harris et al., 2007; Mackay & Leslie, 1987; Mackay et al., 1979; Smith, 1985, 1987). These mechanical methods are convenient but limited to a small area (usually 10 m by 10 m). Leveling surveys have been conducted over a larger area (~400 m by 400 m; Mackay & Burn, 2002). But this method is time-consuming and labor intensive. Recently, new data and methods such as satellite stereo-photogrammetry (Günther et al., 2015; Zwieback et al., 2018), airborne light detection and ranging (Jones et al., 2013; Obu et al., 2017), interferometric synthetic aperture radar (Daout et al., 2017; Liu et al., 2010, 2012), and differential Global Positioning System (GPS; Little et al., 2003; Shiklomanov et al., 2013) have emerged for measuring vertical displacements of frozen ground. All the aforementioned techniques only provide measurements annually or monthly. Limited by the sparse temporal resolution of measurements, a quantitative study on the progressive change of ground elevation during thaw-freeze cycles is lacking.

GPS interferometric reflectometry (GPS-IR) is a new technique that uses the interference of direct and reflected GPS signals for environmental studies (Larson, 2016). The GPS-IR technique has been successfully applied to estimate snow depth (Larson & Nievinski, 2013), sea level changes (Larson, Ray, et al., 2013), soil moisture (Chew et al., 2016), and vegetation water content (Chew et al., 2015). Because the interference between the direct and reflected GPS signals is sensitive to the ground elevation change (related to the distance between the receiver antenna and ground surface), this technique is promising for monitoring ground surface movements over permafrost areas. In a previous study, Liu and Larson (2018) applied GPS-IR to estimate ground subsidence in July and August over 12 summers.

In this study, we construct continuous and consistent GPS-IR records of daily ground elevation changes during snow-free days over a decade at one site in Barrow, Alaska. We focus on interpreting and investigating our observed deformation pattern during the thaw-freeze cycle in one particular year, namely, 2016. Compared with the study of Liu and Larson (2018), our data cover the remaining snow-free days in June and September, which enable us to conduct a more comprehensive study of elevation changes in entire thaw seasons, and more importantly, to reveal, quantify, and understand the frozen ground dynamics during freezing seasons. To our knowledge, this study is not only the first study to use GPS-IR to detect freezing-season ground uplift in a permafrost area but also the first to link the thaw subsidence and freezing uplift as a continuous process at unprecedented, daily intervals. Additionally, we develop a composite physical model that combines climatic thaw and freeze indices to explain these new measurements quantitatively.

2. Study Area and Site Description

Barrow is located on an Arctic coastal plain in the northernmost part of Alaska. This low-relief area is underlain by continuous permafrost with a thickness up to 405 m (Brewer, 1958). The typical vegetation in this area is graminoid-moss tundra. The mean annual air temperature is about −9.7 °C. July is the warmest month with a mean temperature of 4 °C, and February is the coldest month with a mean temperature of −26.4 °C (Streletskiy et al., 2017). The active layer thickness in Barrow is landscape-specific and varies from 29 to 83 cm with an average of 36 cm (Shiklomanov et al., 2010). The thaw season in each year lasts from early June to late August.

In a typical calendar year in Barrow, the snow-free season is shorter than four months, starting from early June to late September or early October when snow starts to accumulate (i.e., snow-in). In 2016, the snow-in occurred in early November, about one month later than in normal years (Cox et al., 2017). This significantly late event opens up a chance for us to use GPS-IR retrieve long records of elevation changes spanning from thaw to freezing season (more in sections 3 and 4).

SG27 is a GPS station (71.3229°N, 156.6103°W) located in northern Barrow with an elevation of ~9 m above sea level (Figure 1a). SG27 is part of the EarthScope Plate Boundary Observatory (PBO) network; with an appropriate azimuth mask, it is usable for GPS-IR (Larson, 2016). The ground around this site is polygon-free upland unaffected by thermokarst processes. The surface soil is silty. SG27 was installed on 4 May 2002 and has been continuously recording GPS signals since then. The GPS antenna is ~3.8 m above the ground surface (Figure 1a), and the bottom of the receiver monument is about 5 m beneath the ground surface.

3. Methodology

3.1. GPS-IR

GPS-IR uses the signal-to-noise ratio (SNR) data as the primary observable to quantify the interference between the reflected and direct signals and estimate the changes of ground reflectors. SNR can be expressed as a sinusoidal equation (Larson, 2016):

$$\mathrm{SNR} = A\cos\left(\frac{4\pi \mathrm{H}}{\lambda}\sin e + \phi\right), \tag{1}$$

where A is the amplitude; H is the reflector height (units: m), which is the vertical distance of the GPS antenna's phase center above the reflecting surface; λ is the wavelength of the GPS signal (units: m); e is the

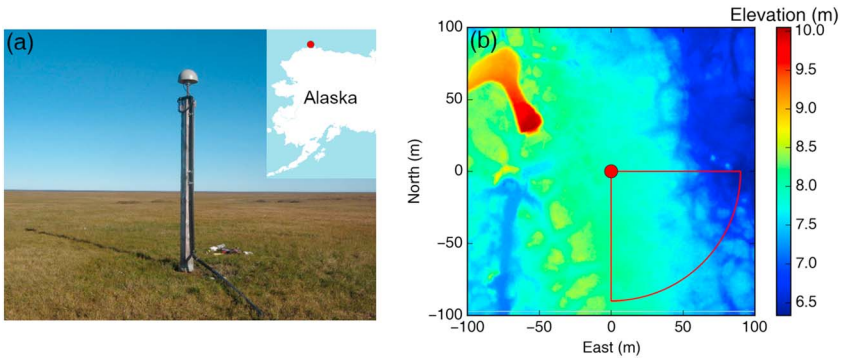

Figure 1. (a) Ground photo viewing the GPS station SG27 toward east on 24 August 2010 (Photo: UNAVCO). The inset shows the location of Barrow (red circle) in Alaska. (b) Relief map of the area surrounding SG27 (marked by the red circle). The red wedge outlines the footprint of the reflected GPS signals.

elevation angle of the satellite; and ϕ is the phase shift. Taking sin (e) as the independent variable, the oscillation frequency f of SNR is $2H/\lambda$.

The retrieval of reflector height in GPS-IR is based on the assumption that the ground is relatively planar and homogeneous within its footprint. We use the same GPS-IR settings (i.e., elevation angle, azimuth range, and L1 signal; λ= 0.190 m) for SG27 as used by Liu and Larson (2018) and estimate a footprint with a radius of 90 m (Larson & Nievinski, 2013), which is shown in Figure 1b. This footprint determined by the specified GPS-IR settings avoids the area with obstructions from man-made structures in the west and north. We retrieve the SNR data versus sin (e) from the observations with a sampling rate of 15 s and determine the reflector height H by using the Lomb-Scargle periodogram analysis (Press et al., 1996). The daily averaged H from all valid satellite tracks is used to represent the reflector height within the footprint. A minimum number of 10 satellite tracks are required to produce a reliable daily average. We calculate the standard error of the mean to represent the uncertainty of the averaged H. Since the anchor of SG27 lies deep in ice-rich permafrost, the changes of reflector heights H are not affected by the solid earth dynamics (Liu & Larson, 2018). The changes of the reflector heights are simply the negative of the changes of ground surface elevation: increase (decrease) of reflector height indicates that the ground subsides (uplifts).

3.2. Composite Model for Seasonal Elevation Changes

To interpret the cyclic pattern of ground elevation changes retrieved by GPS-IR during the thaw-freeze cycle, we propose a composite model based on the response of the active layer to the heat transfer from and to the atmosphere. For a given time t in thaw (freezing) season, the thawing (freezing) depth (Z) of soil can be modeled using the Stefan function (Nelson et al., 1997; Yershov, 1998):

$$Z(t) = \sqrt{\frac{2knA(t)}{\rho\theta L}}, \tag{2}$$

where k is the thermal conductivity of soil (units: $W \cdot m^{-1} \cdot K^{-1}$), n is the n-factor denoting the ratio of ground surface temperatures and air temperatures (Klene et al., 2001; Lunardini, 1978), and $A(t)$ is the accumulated degree days of thaw (units: °C days) for thaw season or accumulated degree days of freezing (units: °C days) for freezing season, calculated using air temperatures. In this study, we calculate accumulated degree days of thaw and accumulated degree days of freezing using the daily averaged 2-m air temperatures measured at the National Oceanic and Atmospheric Administration Barrow Observatory; ρ is the soil bulk density (units: kg/m^3), θ is the volumetric water content (units: m^3/m^3), and L is the specific latent heat of fusion for water (units: J/kg). Throughout this paper, we use the superscripts "T" and "F" to represent the thaw season and freezing season, respectively.

The phase change of water causes the volume change of soil within the thawing (freezing) depth. During the freezing process, an incremental layer of the unfrozen soil with thickness of dz freezes within time dt. We

assume that all the pore water within this frozen layer turns into ice, which causes an ~9% volume increase and the ground uplifts accordingly, by *du*:

$$du = \frac{\rho_w - \rho_i}{\rho_i}\theta dz, \tag{3}$$

where ρ_w and ρ_i are the density of pure water and pure ice, respectively. Assuming that the soil is homogeneous with constant water content (i.e., θ is invariant with depth), we substitute equation (3) into equation (2) and rearrange the equation:

$$u(t) = \frac{\rho_w - \rho_i}{\rho_i}\sqrt{\frac{2k_F\, n_F\, \theta A_F(t)}{\rho L}}, \tag{4}$$

where $u(t)$ is the time-variant ground uplift (units: m). Introducing a time-invariant coefficient:

$$E_F = \frac{\rho_w - \rho_i}{\rho_i}\sqrt{\frac{2k_F\, n_F \theta}{\rho L}}, \tag{5}$$

we derive a simple square-root relationship between the uplift and freeze index:

$$u(t) = E_F\sqrt{A_F(t)}. \tag{6}$$

The coefficient E_F is the seasonal coefficient of uplift (units: m (°C days)$^{-1/2}$). Using a similar manner, we can derive the subsidence due to melting of pore ice during the thaw season as $s(t) = E_T\sqrt{A_T(t)}$ with the seasonal coefficient:

$$E_T = \frac{\rho_w - \rho_i}{\rho_i}\sqrt{\frac{2k_T\, n_T\theta}{\rho L}}. \tag{7}$$

We simplify the annual thaw-freeze cycle as a consecutive year from the beginning of the thaw season to the beginning of the next thaw season. To create a deformation model incorporating both thaw settlement and freezing uplift, we assume that the elevation *d* at any given time *t* during the annual thaw-freeze cycle is a balance between thawing and freezing. Then we can get

$$d(t) = s(t) - u(t) = E_T\sqrt{A_T(t)} - E_F\sqrt{A_F(t)}. \tag{8}$$

Furthermore, the two seasonal coefficients E_F and E_T can be related by a scaling factor α:

$$\alpha = \frac{E_F}{E_T} = \sqrt{\frac{k_F\, n_F}{k_T\, n_T}}. \tag{9}$$

To determine the scaling factor α in Barrow, we use the thermal conductivities (k_F=1.4 W · m^{-1} · K^{-1}, k_T=0.6 W · m^{-1} · K^{-1}) as estimated by Romanovsky and Osterkamp (2000) and the *n*-factors (n_F= 0.73, n_T= 0.82) given by related research studies (Hinkel et al., 2008; Klene et al., 2001). Thus, the scaling factor α specific for Barrow is 1.44.

Then we introduce a composite index $I_c(t)$ to combine the thaw and freeze indices as

$$I_c(t) = \sqrt{A_T(t)} - \alpha\sqrt{A_F(t)}. \tag{10}$$

Finally, we arrive at a simple composite model for seasonal elevation changes due to thawing/freezing of the active layer:

$$d(t) = E_T I_c(t). \tag{11}$$

For an annual thaw-freeze cycle, we set the composite index to be zero after the timing of the completely frozen of the active layer when $\sqrt{A_T(t)} = \alpha\sqrt{A_F(t)}$, and from then we assume that there are no elevation changes until the onset of the next thaw season.

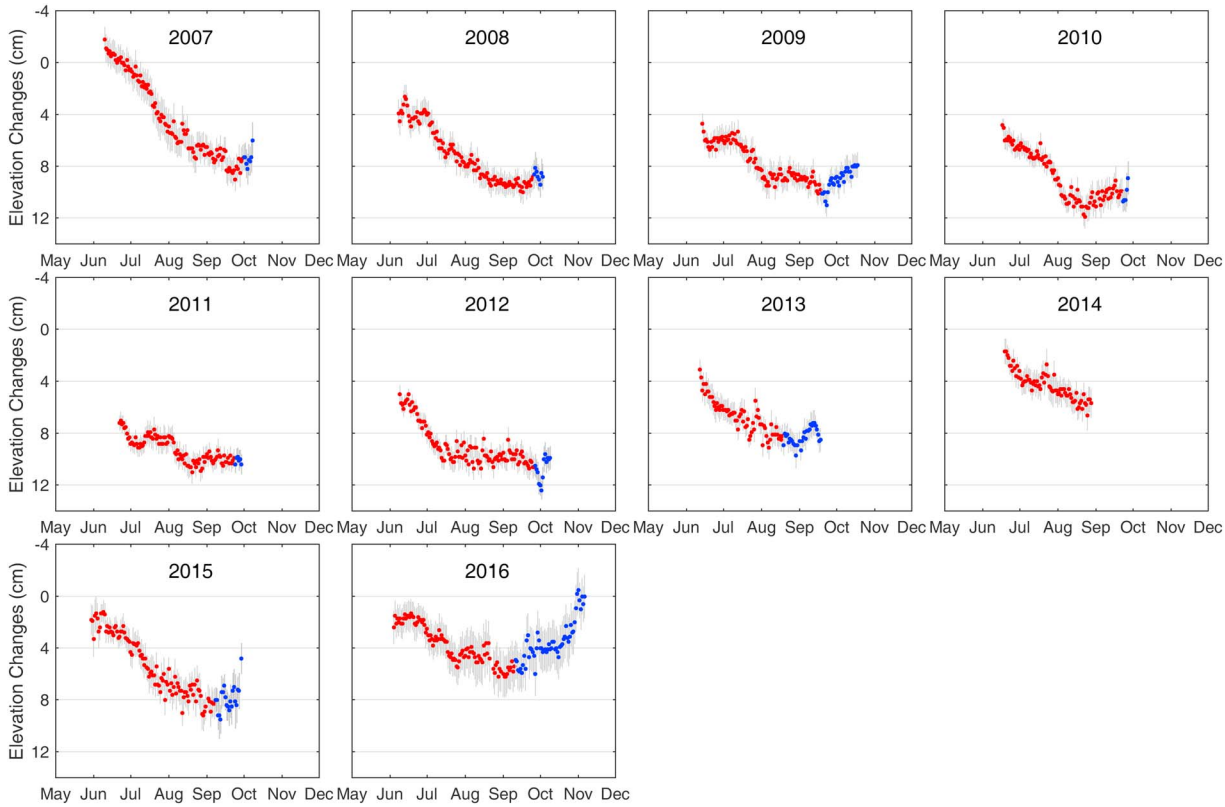

Figure 2. Time series of daily elevation changes on snow-free days from 2007 to 2016. The red dots and blue dots represent the thaw and freezing seasons, respectively. The gray error bars represent the uncertainties of the elevation changes. The 2016 time series is identical to those shown in Figures 3a and 4b.

3.3. Fitting Composite Model to Observed Elevation Changes

Because we are only interested in characterizing the temporal pattern of elevation changes, we normalize the composite index with its maximum value and modify equation (11) to a more general linear function:

$$d(t) = d_s \tilde{I}_c(t) + d_0, \tag{12}$$

where d_s is the maximum seasonal deformation (units: m), $\tilde{I}_c$ is the normalized I_c by its maximum value, and d_0 is the reference elevation. For convenience, we select the highest elevation during the snow-free days as the reference value to calculate the elevation changes. Finally, given GPS-IR-retrieved $d(t)$ and its uncertainties (i.e., data), and $\tilde{I}_c(t)$ calculated from air temperatures (i.e., variables), we use the weighted least squares method to fit the composite model to the data. Equation (12) is a linear model, so we only need to fit two linear coefficients: d_s and d_0.

4. Results

Figure 2 shows the cyclic ground elevation changes derived by GPS-IR on snow-free days in each year from 2007 to 2016. The ground surface underwent gradual and progressive subsidence during each thaw season from June to around September. Because of the snow precipitation in fall, the records of uplifts following the subsidence were relatively short in most years (the records were the longest in 2016). The records in 2014 were the shortest because the first snow-in was the earliest (30 August) and 25 days earlier than the onset of freezing. From these, we observe the same interannual and decadal variability as Liu and Larson (2018). In the remainder of this paper, we will focus on presenting, interpreting, and discussing the seasonal, cyclic elevation changes in 2016. Liu and Larson (2018) gave a more detailed and in-depth interpretation of the interannual and decadal variability.

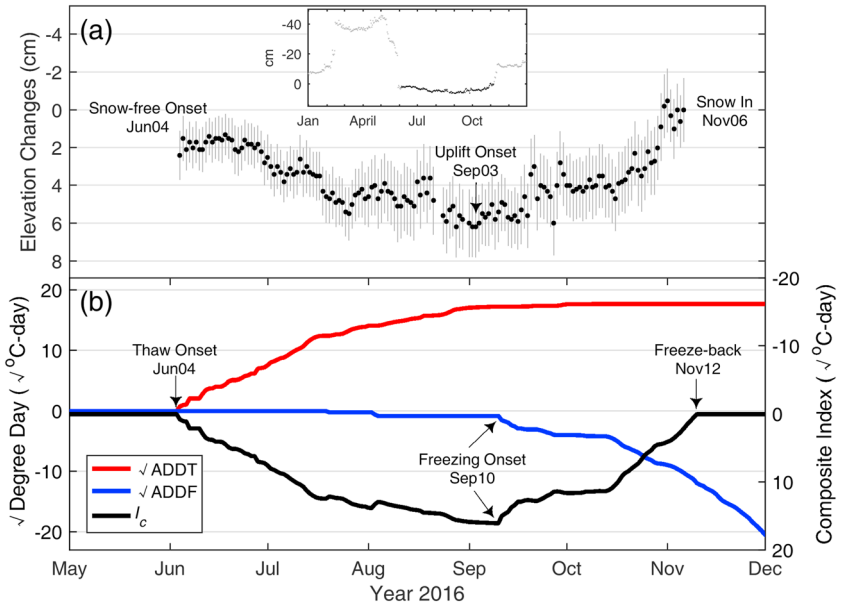

Figure 3. (a) Time series of elevation changes at SG27 on snow-free days in 2016. The gray error bars represent the uncertainties of daily average elevation changes. The inset shows the elevation changes spanning the calendar year of 2016 with the gray dots showing the snow-covered days. (b) Time series of $\sqrt{A_T}$ and $\sqrt{A_F}$, as well as the composite index I_c. Note that the vertical axis of the composite index plot is flipped to facilitate comparison with the elevation change plot (i.e., Figure 3a).

Figure 3 shows the ground elevation changes and thermal indices for 2016, the year with the longest snow-free period. The elevation changes were dominated by changes in snow depth during the snow-covered days (Figure 3a, inset). From 4 June to 6 November, the changes of reflector heights were mainly caused by the elevation changes of the ground surface. Specifically, the ground surface first subsided for about 92 days from 4 June to 3 September during the thaw season, followed by an uplift for about 64 days from 4 September to 6 November during the freezing season. Moreover, the net uplift in the freezing season was roughly equal to the net subsidence in the preceding thaw season.

Figure 3b shows the time series of the thaw index (in forms of $\sqrt{A_T}$), freeze index (in forms of $\sqrt{A_F}$), and composite index (I_c). As indicators of the thaw onset, $\sqrt{A_T}$ and I_c started to increase on 11 May, when the air temperature rose above 0 °C. However, the above-zero temperature lasted for only three days and dropped below 0 °C till 4 June (Figure S1 in the supporting information). Taking this into account, we determine 4 June as the thaw onset. On 10 September, I_c reached to its maximum value and the freeze index started to increase, indicating the end of the thaw, which is also the freezing onset. I_c dropped back to zero on 12 November, representing the complete freeze-back of the active layer. In general, the dates determined by thermal indices using the air temperature and GPS-IR measurements agreed within seven days. Additionally, we compared these dates determined from indices with ground temperatures at depth of 1 cm (Figure S1) measured at a nearby borehole site coded "Barrow 2" (~2.4 km southwest of SG27). The ground temperature records suggest 3 June as the thaw onset and 12 September as the freezing onset as both were close to the index-based dates.

The fitting results for 2016 and the other years are shown in Figures 4a and S2, respectively. The composite model fits the elevation changes very well, with R^2 values ranging from 0.69 to 0.94 (0.79 for 2016) and a mean of 0.79 for all 10 years. In 2016, the fitting suggests a seasonal amplitude of 5.1 ± 0.2 cm.

We also examine the fitting by directly overlapping the time series of the elevation changes with the best fit composite model. We observe a high level of matching between the best fit composite model and the elevation changes (Figure 4b for 2016 and Figure S3 for the other years). We also note an abnormal, temporary thaw-season heave coincided with the temporary changes depicted by the composite model in early August (marked by the magenta box in Figure 4b). Such temporary uplift in thaw season indicates transient summer freezing. This is a new feature attributed to the combination of thaw and freeze indices in the

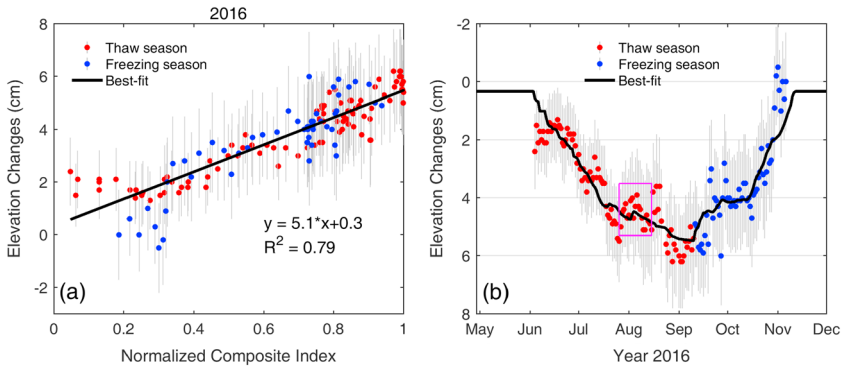

Figure 4. (a) Scatter plot between the GPS-IR-retrieved elevation changes and the normalized composite indices. The red and blue dots represent the elevation changes in thaw and freezing seasons, respectively. The error bars denote the uncertainties of elevation changes. The black line shows the linear fitting. The linear fitting formula and corresponding R^2 value are displayed. (b) Time series of the elevation changes (dots) and the best fit composite model (black line). The magenta box marks an abnormal heave during the thaw season.

composite model. It is a key improvement over the previous simple model of Liu et al. (2012), which uses only a single thaw index.

5. Discussion

Our GPS-IR results reveal the ground elevation evolution from thaw season to freezing season. During the thaw season, the ground surface gradually subsides with the heat transporting downward from the surface driving the thawing of the soil. This one-side thawing caused by thermal conduction associated with phase change can be well modeled using the Stefan function (i.e., equation (2)), reflecting the thermal response of the active layer to the atmospheric forcing. The sudden drop of temperature below 0 °C occurred in early August of 2016 temporarily froze the ground, resulting in the temporary heave in the summer. At the end of thaw season (also the freezing onset), the ground subsidence reached to its maximum value with the maximum thawing depth. From then on, air temperature dropped below 0 °C and the active layer began to refreeze. During the freezing season of 2016, the ground surface continuously uplifted with freezing downward from the surface. Due to the larger thermal conductivity and faster changes of the atmospheric forcing represented by the thermal index in freezing season (Figure 3b), the heat transport is more intensive in freezing season than that in thaw season, contributing to the faster freezing heave than the thaw settlement (Figure 3a). Driven by the thaw-freeze cycle of the active layer, the ground surface underwent cyclic deformation, whose amplitude is quantified by the GPS-IR-derived elevation changes fitted with the composite model (i.e., equation (12)).

Our composite model well explains the general pattern of cyclic ground elevation changes on snow-free days. This composite model is simple and only needs temperature information. Therefore, it can be easily included in complex, regional, or global permafrost models to account for surface elevation changes. However, this simple model has a few limitations. First, the composite index only considers the seasonal elevation changes of frozen ground. Any interannual or decadal changes due to the aggradation or degradation of permafrost are not included in equation (11). Second, we use the air temperature instead of the ground surface temperature in the composite model. One reason is that air temperature records are much more accessible than ground temperatures. Another reason for using air temperature is to avoid the "zero curtain" effects (Figure S1). Zero curtain refers to a phenomenon that the specific portion of the active layer maintains a temperature near 0 °C when the soil water is freezing to ice and it lasts until freezing is complete (Outcalt et al., 1990). Because water is freezing into ice during the zero curtain, it would still result in surface uplift despite the invariant ground temperature. However, if ground temperature were used to calculate the composite model, we would obtain a constant composite index during the zero curtain and predict no changes in surface elevation. Such a prediction is contradictory to the significant uplift revealed by our GPS-IR measurements. Third, in the simple composite model, we assume that the ground uplift during the early-winter freezing is caused by the local freezing of pore water to pore ice. This "in situ" uplift is not "frost heave" caused by

the formation of segregated ice (ice lenses), a much more complicated process than what is described by equation (11). One can evaluate the frost heave by the model considering different regimes of the ice-lens formation (e.g., Rempel, 2007). However, the sophisticated model may or may not be relevant to the freezing-period uplift in early winter.

6. Conclusions

This study is the first attempt to use the GPS-IR technique to obtain continuous records of ground elevation changes from thaw to freezing season in a permafrost area. Our daily GPS-IR measurements at Barrow reveal clear, cyclic pattern of subsidence followed by uplift through the thaw and freezing seasons. We show that the GPS-IR technique can be used to monitor frozen ground movements consistently and continuously from thaw to freezing season and with great detail. This means that daily GPS-IR measurements can complement ongoing permafrost observations by filling temporal and spatial gaps. In future, more investigations by GPS-IR at other GPS sites located in permafrost areas are necessary to explore the spatiotemporal dynamics of thaw subsidence and freezing uplift. Here we have introduced a new composite model for seasonal elevation changes that includes contributions from both thawing and freezing. It shows good agreement with the GPS-IR measurements. Its simplicity suggests great potential for applying this model for other permafrost studies and models.

Acknowledgments
We thank John Wahr for inspiring this research and Christopher Cox and Robert Stone for providing the snow data collected at the NOAA Barrow Observatory. We thank two anonymous reviewers for their insightful comments and constructive suggestions. The raw Plate Boundary Observatory GPS data collected by SG27 are available from UNAVCO (http://pbo.unavco.org). Data generated in this study are available at https://doi.pangaea.de/10.1594/PANGAEA.884941. The work at The Chinese University of Hong Kong was supported by Hong Kong Research Grants Council (CUHK24300414 and CUHK14300815) and CUHK Direct Grants for Research (4053206). K. M. Larson was supported by NSF AGS 1449554. K. M. Schaefer was supported by NASA grant NNX17AC59A as part of the Arctic Boreal Vulnerability Experiment.

References

Brewer, M. C. (1958). Some results of geothermal investigations of permafrost in northern Alaska. *Transactions of the American Geophysical Union*, *39*(1), 19. https://doi.org/10.1029/tr039i001p00019

Chew, C., Small, E. E., & Larson, K. M. (2016). An algorithm for soil moisture estimation using GPS-interferometric reflectometry for bare and vegetated soil. *GPS Solutions*, *20*(3), 525–537. https://doi.org/10.1007/s10291-015-0462-4

Chew, C. C., Small, E. E., Larson, K. M., & Zavorotny, V. U. (2015). Vegetation sensing using GPS-interferometric reflectometry: Theoretical effects of canopy parameters on signal-to-noise ratio data. *IEEE Transactions on Geoscience and Remote Sensing*, *53*(5), 2755–2764. https://doi.org/10.1109/tgrs.2014.2364513

Cox, C. J., Stone, R. S., Douglas, D. C., Stanitski, D. M., Divoky, G. J., Dutton, G. S., et al. (2017). Drivers and environmental responses to the changing annual snow cycle of northern Alaska. *Bulletin of the American Meteorological Society*, *98*(12), 2559–2577. https://doi.org/10.1175/bams-d-16-0201.1

Daout, S., Doin, M. P., Peltzer, G., Socquet, A., & Lasserre, C. (2017). Large-scale InSAR monitoring of permafrost freeze-thaw cycles on the Tibetan Plateau. *Geophysical Research Letters*, *44*, 901–909. https://doi.org/10.1002/2016GL070781

Günther, F., Overduin, P. P., Yakshina, I. A., Opel, T., Baranskaya, A. V., & Grigoriev, M. N. (2015). Observing Muostakh disappear: Permafrost thaw subsidence and erosion of a ground-ice-rich island in response to arctic summer warming and sea ice reduction. *The Cryosphere*, *9*(1), 151–178. https://doi.org/10.5194/tc-9-151-2015

Harris, C., Luetschg, M., Davies, M. C., Smith, F., Christiansen, H. H., & Isaksen, K. (2007). Field instrumentation for real-time monitoring of periglacial solifluction. *Permafrost and Periglacial Processes*, *18*(1), 105–114. https://doi.org/10.1002/ppp.573

Hinkel, K. M., Klene, A. E., & Nelson, F. E. (2008). Spatial and interannual patterns of winter n-factors near Barrow, Alaska. In *Proceedings of the Ninth International Conference on Permafrost* (Vol. 28, pp. 705–709). Fairbanks, AK: Institute of Northern Engineering, University of Alaska Fairbanks.

Jones, B. M., Stoker, J. M., Gibbs, A. E., Grosse, G., Romanovsky, V. E., Douglas, T. A., et al. (2013). Quantifying landscape change in an arctic coastal lowland using repeat airborne LiDAR. *Environmental Research Letters*, *8*(4), 045025. https://doi.org/10.1088/1748-9326/8/4/045025

Klene, A. E., Nelson, F. E., Shiklomanov, N. I., & Hinkel, K. M. (2001). The n-factor in natural landscapes: Variability of air and soil-surface temperatures, Kuparuk River Basin, Alaska, USA. *Arctic, Antarctic, and Alpine Research*, *33*(2), 140–148. https://doi.org/10.2307/1552214

Larson, K. M. (2016). GPS interferometric reflectometry: Applications to surface soil moisture, snow depth, and vegetation water content in the western United States. *Wiley Interdisciplinary Reviews: Water*, *3*(6), 775–787. https://doi.org/10.1002/wat2.1167

Larson, K. M., & Nievinski, F. G. (2013). GPS snow sensing: Results from the EarthScope Plate Boundary Observatory. *GPS Solutions*, *17*(1), 41–52. https://doi.org/10.1007/s10291-012-0259-7

Larson, K. M., Ray, R. D., Nievinski, F. G., & Freymueller, J. T. (2013). The accidental tide gauge: A GPS reflection case study from Kachemak Bay, Alaska. *IEEE Geoscience and Remote Sensing Letters*, *10*(5), 1200–1204. https://doi.org/10.1109/lgrs.2012.2236075

Little, J. D., Sandall, H., Walegur, M. T., & Nelson, F. E. (2003). Application of differential global positioning systems to monitor frost heave and thaw settlement in tundra environments. *Permafrost and Periglacial Processes*, *14*(4), 349–357. https://doi.org/10.1002/ppp.466

Liu, L., & Larson, K. M. (2018). Decadal changes of surface elevation over permafrost area estimated using reflected GPS signals. *The Cryosphere*, *12*(2), 477–489. https://doi.org/10.5194/tc-12-477-2018

Liu, L., Schaefer, K., Zhang, T., & Wahr, J. (2012). Estimating 1992–2000 average active layer thickness on the Alaskan North Slope from remotely sensed surface subsidence. *Journal of Geophysical Research*, *117*, F01005. https://doi.org/10.1029/2011JF002041

Liu, L., Zhang, T., & Wahr, J. (2010). InSAR measurements of surface deformation over permafrost on the North Slope of Alaska. *Journal of Geophysical Research*, *115*, F03023. https://doi.org/10.1029/2009JF001547

Lunardini, V. (1978, July). Theory of n-factors and correlation of data. In *Proceedings of the Third International Conference on Permafrost* (Vol. 1, pp. 40–46). Ottawa: National Research Council of Canada.

Mackay, J. R., & Burn, C. R. (2002). The first 20 years (1978-1979 to 1998-1999) of active-layer development, Illisarvik experimental drained lake site, western Arctic coast, Canada1. *Canadian Journal of Earth Sciences*, *39*(11), 1657–1674. https://doi.org/10.1139/e02-068

Mackay, J. R., & Leslie, R. V. (1987). A simple probe for the measurement of frost heave within frozen ground in a permafrost environment. Current research, part A. Geological Survey of Canada (pp. 37–41). https://doi.org/10.4095/122503

Mackay, J. R., Ostrick, J., Lewis, C. P., & MacKay, D. K. (1979). Frost heave at ground temperatures below 0 C, Inuvik, Northwest Territories. Geological Survey of Canada Paper (pp. 403–406).

Nelson, F. E., Shiklomanov, N. I., Mueller, G. R., Hinkel, K. M., Walker, D. A., & Bockheim, J. G. (1997). Estimating active-layer thickness over a large region: Kuparuk River basin, Alaska, USA. *Arctic and Alpine Research*, *29*(4), 367–378. https://doi.org/10.2307/1551985

Obu, J., Lantuit, H., Grosse, G., Günther, F., Sachs, T., Helm, V., & Fritz, M. (2017). Coastal erosion and mass wasting along the Canadian Beaufort Sea based on annual airborne LiDAR elevation data. *Geomorphology*, *293*, 331–346. https://doi.org/10.1016/j.geomorph.2016.02.014

Outcalt, S. I., Nelson, F. E., & Hinkel, K. M. (1990). The zero-curtain effect: Heat and mass transfer across an isothermal region in freezing soil. *Water Resources Research*, *26*, 1509–1516. https://doi.org/10.1029/90WR00139

Press, W. H., Teukolsky, S. A., Vetterling, W. T., & Flannery, B. P. (1996). *Numerical recipes in Fortran 90: The art of parallel scientific computing*, (2nd ed.). Cambridge: Cambridge University Press.

Rempel, A. W. (2007). Formation of ice lenses and frost heave. *Journal of Geophysical Research*, *112*, F02S21. https://doi.org/10.1029/2006JF000525

Romanovsky, V. E., & Osterkamp, T. E. (2000). Effects of unfrozen water on heat and mass transport processes in the active layer and permafrost. *Permafrost and Periglacial Processes*, *11*(3), 219–239. https://doi.org/10.1002/1099-1530(200007/09)11:3<219::aid-ppp352>3.0.co; 2–7

Shiklomanov, N. I., Streletskiy, D. A., Little, J. D., & Nelson, F. E. (2013). Isotropic thaw subsidence in undisturbed permafrost landscapes. *Geophysical Research Letters*, *40*, 6356–6361. https://doi.org/10.1002/2013GL058295

Shiklomanov, N. I., Streletskiy, D. A., Nelson, F. E., Hollister, R. D., Romanovsky, V. E., Tweedie, C. E., et al. (2010). Decadal variations of active-layer thickness in moisture-controlled landscapes, Barrow, Alaska. *Journal of Geophysical Research*, *115*, G00I04. https://doi.org/10.1029/2009JG001248

Smith, D. J. (1987). Frost-heave activity in the Mount Rae area, Canadian Rocky Mountains. *Arctic and Alpine Research*, *19*(2), 155–166. https://doi.org/10.2307/1551248

Smith, M. W. (1985). Observations of soil freezing and frost heave at Inuvik, Northwest Territories, Canada. *Canadian Journal of Earth Sciences*, *22*(2), 283–290. https://doi.org/10.1139/e85-024

Streletskiy, D. A., Shiklomanov, N. I., Little, J. D., Nelson, F. E., Brown, J., Nyland, K. E., & Klene, A. E. (2017). Thaw subsidence in undisturbed tundra landscapes, Barrow, Alaska, 1962–2015. *Permafrost and Periglacial Processes*, *28*(3), 566–572. https://doi.org/10.1002/ppp.1918

Yershov, E. D. (1998). *General Geocryology*. Cambridge: Cambridge University Press. https://doi.org/10.1017/CBO9780511564505

Zwieback, S., Kokelj, S. V., Günther, F., Boike, J., Grosse, G., & Hajnsek, I. (2018). Sub-seasonal thaw slump mass wasting is not consistently energy limited at the landscape scale. *The Cryosphere*, *12*(2), 549–564. https://doi.org/10.5194/tc-12-549-2018